Ocean Engineering 340 (2025) 122307

Contents lists available at ScienceDirect

Ocean Engineering

journal homepage: www.elsevier.com/locate/oceaneng

Research paper

A novel coupling framework for integrating turbine and substructure dynamics of floating offshore wind turbines

Yanfei Deng [a], Cuizhi Zhu [a], Sara Ying Zhang [b], Yifeng Yang [c,*], Bingfu Zhang [a]

[a] School of Intelligence, Harbin Institute of Technology Shenzhen, Shenzhen, 518000, Guangdong, China
[b] School of Electromechanical Engineering, Guangdong University of Technology, Guangzhou, 510000, Guangdong, China
[c] Department of Mechanical Engineering, University College London, Torrington Place, London, WC1E 7JE, United Kingdom

ARTICLE INFO

Keywords:
Floating offshore wind turbine
Coupling interface
OpenFAST
Orcaflex

ABSTRACT

This study presents OrcaWind, a novel aero-hydro-servo-elastic coupling framework that seamlessly integrates OpenFAST and OrcaFlex to address critical limitations of single-tool approaches in floating offshore wind turbine (FOWT) simulations. By synergizing OrcaFlex's superior modeling capacities in hydrodynamics and multi-body system with OpenFAST's validated aerodynamic methodologies, the framework enables efficient and accurate multi-physics simulations. Rigorous validation against OpenFAST benchmarks confirms its accuracy in predicting coupled dynamic responses, including servo-control behaviors, aerodynamic loads, platform motions, and mooring tensions. A case study of a 15 MW FOWT with a constant tension mooring system (CTMS) further demonstrates OrcaWind's unique capability to evaluate complex platform-mooring interactions. By contrast to conventional tools, the framework explicitly resolves nonlinear mooring line dynamics, delivering more reliable and comprehensive dynamic assessments. These advancements establish OrcaWind as an advanced tool for optimizing FOWTs with innovative substructures or mooring configurations. The framework will be publicly released following article publication to support offshore wind energy development.

1. Introduction

Floating offshore wind turbines (FOWTs) offer significant advantages over traditional fixed-bottom wind turbines. They can access vast offshore wind resources in deep waters, avoid sensitive coastal areas, and minimize impacts on marine ecosystems. FOWT technology has advanced considerably since its debut in 2009 with a pilot 2 MW turbine in Norway (Hau, 2013). Currently, the world's largest floating offshore wind farm, with a capacity of 1 GW, is under construction off the coast of Wanning (Enerdata, 2023). According to DNV's Energy Transition Outlook 2022 (DNV, 2022), the cumulative installed capacity of FOWTs is expected to reach 300 GW by 2050. In recent years, the industry has been actively developing and demonstrating innovative concepts (Leimeister, 2022; Terrero-Gonzalez et al., 2024; Xie et al., 2025) to reduce the high development costs, which remain the biggest barrier to their large-scale application. Therefore, accurate and efficient simulation tools that can accommodate various designs are essential for the development of FOWTs (Lauria et al., 2024).

In contrast to floating offshore oil and gas platform, FOWTs have tall turbine structures with significant wind-induced loads. The aerodynamic loads are influenced not only by wind speed and direction but also by the motion of the floating structure and the servo behavior (Deng et al., 2023). Additionally, there is a notable disparity in the structural stiffness of FOWT subsystems (Lamei et al., 2025). While the floating platform is typically treated as a rigid body, the blades and towers of large megawatt turbines exhibit a certain degree of flexibility, and the mooring system and dynamic cables are considered flexible structures. Consequently, FOWTs are multi-source excited coupled systems with significant nonlinearity and coupling characteristics in their dynamic behavior. Fully coupled aero-hydro-servo-elastic models are widely accepted for providing reliable dynamic responses predictions (Lei et al., 2021).

Several simulation tools have been developed in both academia and industry (Otter et al., 2022), including Bladed, HAWC2, and OpenFAST (the successor to FAST), as well as various in-house programs (López-Queija et al., 2024). Most of these tools are based on similar theoretical frameworks (Faraggiana et al., 2022). For aerodynamic modeling, the Blade Element Momentum (BEM) theory and its

This article is part of a special issue entitled: OWF Frontiers published in Ocean Engineering.

* Corresponding author.
E-mail address: yifeng.yang.19@ucl.ac.uk (Y. Yang).

https://doi.org/10.1016/j.oceaneng.2025.122307
Received 26 March 2025; Received in revised form 15 July 2025; Accepted 26 July 2025
Available online 1 August 2025
0029-8018/© 2025 The Authors. Published by Elsevier Ltd. This is an open access article under the CC BY license (http://creativecommons.org/licenses/by/4.0/).

associated correction models are commonly used. In hydrodynamics, 3D potential flow theory and Morison equation are widely applied. Blade structural responses are typically modeled using modal analysis, geometrically exact beam models, and multibody dynamics models. Mooring system responses are usually modeled with catenary equations, lumped mass methods, or finite element methods. However, due to the diverse designs and varying focuses of FOWTs, existing numerical tools still have certain limitations. For instance, OpenFAST and Bladed lack some hydrodynamic capabilities that are available in offshore engineering software like Orcaflex. Although Orcaflex has developed its own wind turbine module for independent coupled analysis, its aerodynamic and aeroelastic algorithms are limited and offer fewer options.

Integrating diverse modules with superior capabilities from various sources is an effective strategy for enhancing the coupled analysis of FOWTs. For instance, SIMO-Riflex-AeroDyn combines SIMO's multibody dynamics with Riflex's nonlinear beam and bar deformation and AeroDyn's aerodynamic capabilities (Luan et al., 2017). CHARM3D-FAST integrates CHARM3D's hydrodynamic models with FAST's aerodynamic and control features, offering robust coupled analysis capabilities (Bae and Kim, 2014). Other initiatives, such as F2A, merge the wind turbine dynamics of FAST with AQWA's hydrodynamic modeling (Yang et al., 2020). Similarly, Orcina developed C/C++-based FASTlink to integrate FAST's aerodynamic strengths with Orcaflex's hydrodynamic capabilities via a dynamic link library (DLL) interface (Orcina, 2023). While FASTlink allows FAST to access the hydrodynamic loads, the 6-dof motion responses of the floating platform are solved within FAST, leading to limitations such as the inability to model shared mooring systems (Tian et al., 2025; Xie et al., 2024), dual rotor designs (Bolat et al., 2025; Shen et al., 2024), or T-Omega design configurations (Terrero-Gonzalez et al., 2024). Additionally, when using FASTlink, considerations must be taken to avoid reference frame misalignment, double-counting of gravitational forces, inconsistent time-stepping, and imbalance in initial conditions (Masciola et al., 2011).

To address the aforementioned issues, this study develops a novel aero-hydro-servo-elastic coupling framework, OrcaWind, which integrates OpenFAST and Orcaflex. This coupling framework is achieved by modifying and compiling OpenFAST into a DLL, and integrating it with Orcaflex via Python codes to obtain aerodynamic loads. It is designed to enhance FOWT dynamics simulation and offers several key advantages. First, it provides access to various aerodynamic and aeroelastic algorithms within OpenFAST. Second, it can simulate a range of innovative floating offshore wind turbine concepts. Third, it offers greater flexibility in time-step settings, enabling more efficient large-step implicit calculations for hydrodynamics.

The remainder of the paper is structured as follows. Section 2 presents the key methodologies and technical details underlying the development of the OrcaWind framework. Section 3 rigorously validates the framework's accuracy and reliability through comprehensive comparative analyses with OpenFAST simulations. In Section 4, a case study investigating a FOWT equipped with a constant tension mooring system (CTMS) demonstrates the framework's superior capability in simulating novel floating platform and mooring configurations. Finally, Section 5 summarizes the principal findings and conclusions.

2. Methodology and modeling

The OrcaWind framework achieves seamless aero-hydro-servo-elastic coupling through algorithmic modification and dynamic compilation of OpenFAST into a DLL, referred as FASTDLL below. The FASTDLL interfaces with Orcaflex via a Python-mediated external function interface. The framework leverages OrcaFlex's efficient modeling of floater dynamics and mooring system responses, while delegating turbine-specific simulations, including aerodynamic loading, structural deformation, and control system behavior, to the embedded FASTDLL.

2.1. Wind turbine modeling in OpenFAST

OpenFAST, an open-source multiphysics simulation platform developed by the National Renewable Energy Laboratory (NREL), providing comprehensive modeling capabilities for coupled dynamic analysis of wind turbine systems (NREL, 2021). Its modular architecture and open-source accessibility facilitate seamless integration and customization, making it particularly advantageous for research-oriented secondary development. Among all the modules, the essential module—AeroDyn for aerodynamic analysis, ElastoDyn for structural dynamics, and ServoDyn for control systems—form the core components enabling these simulations.

AeroDyn incorporates three distinct wake modeling methodologies: the Blade Element Momentum (BEM) theory, the Generalized Dynamic Wake (GDW) model, and the Convecting Lagrangian Filaments (OLAF) approach (Jonkman et al., 2015). Each methodology integrates with a dynamic stall model based on the semi-empirical Beddoes-Leishman formulation to compute blade element loading. The BEM method, a classical approach in rotor aerodynamics, calculates induced velocities from axial and tangential momentum lost, which requires correction models for tip/hub losses and skewed wakes to enhance the accuracy. By contrast, the GDW methodology inherently incorporates these phenomena through the potential flow solutions derived from the Laplace equation, utilizing Legendre expansions to characterize rotor-plane pressure distributions. Notably, GDW reverts to BEM approximations under low-wind conditions due to its underlying assumption of small induced velocities and exclusion of wake rotation effects. For scenarios involving significant blade deformations and platform-induced rotor motions, the OLAF method offers a computationally efficient alternative through its Lagrangian-based free vortex wake formulation, bridging the gap between engineering models and high-fidelity CFD approaches. All these wake models are utilized to calculate the induced velocities and determine the angle of attack on blade elements. For our study, the BEM model was adopted due to its computational efficiency for coupled global performance assessment, aligning with our focus on aero-hydrodynamic coupling rather than detailed near-wake aerodynamics.

Fig. 1 illustrates the velocity components and corresponding aerodynamic loads acting on a blade element, where Ω represents the rotor angular velocity and r denotes the local radial position of the blade element. a and a' are the axial and tangential induction factors, $v_{e\text{-}ip}$ and $v_{e\text{-}op}$ are in plane and out-of-plane element velocities due to blade motion. Key aerodynamic parameters include the angle of attack (α), blade twist (β), inflow angle (ϕ), along with the inflow velocity (V_∞) and resultant velocity (V_{total}). The elemental lift (L) and drag (D) forces are derived from airfoil aerodynamic coefficients, enabling calculation of the aerodynamic thrust dT and torque dM on each element through Eq. (1) and Eq. (2).

$$dT = \frac{1}{2}\rho V_{total}^2 (C_l \cos\varphi + C_d \sin\varphi) c dr \tag{1}$$

$$dM = \frac{1}{2}\rho V_{total}^2 (C_l \sin\varphi - C_d \cos\varphi) c r dr \tag{2}$$

where C_l and C_d correspond to the sectional lift and drag coefficients, respectively, and c indicates the local chord length. At each time step, AeroDyn is called by ElastoDyn to calculate the aerodynamic forces, which affect the blade deflections and motions, and vice versa.

ElastoDyn employs Kane's dynamic formulation to establish governing equations for wind turbine structural dynamics, encompassing blade-tower-nacelle interactions. The methodology initiates by defining generalized coordinates and velocities, followed by systematic derivation of generalized active forces (F_r) and inertial forces (F_r^*) through Kane's equations, ultimately yielding the compact matrix form:

$$F_r + F_r^* = 0 \quad (r = 1, \cdots, n) \tag{3}$$

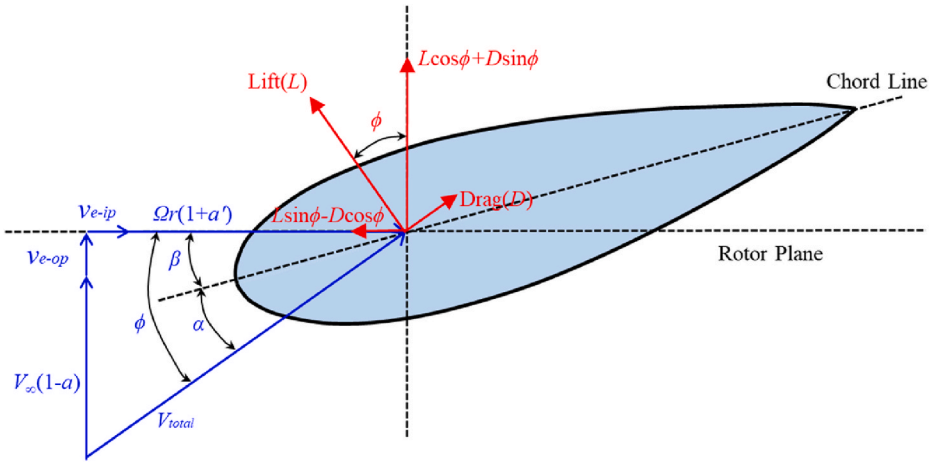

Fig. 1. Local velocities and aerodynamic loads of a blade element (Moriarty, 2005).

The limited, prescribed DOFs in ElastoDyn (Guo et al., 2024), while computationally efficient, constrains the modeling flexibility for innovative structural designs. In this study, the original motion solver in ElastoDyn was replaced with displacement-driven boundary conditions, removing floater 6-dof motions from the solution matrix and instead prescribing them via kinematic inputs received from OrcaFlex at each time step.

The operational envelope regulation via variable-speed and collective pitch control constitutes a critical subsystem for performance optimization and load alleviation. ServoDyn provides an integration for modular controller implementation, notably supporting industry-standard Bladed-style DLL controllers such as ROSCO. Its standard architecture comprises three core components: (1) sensor signal conditioning filters, (2) generator torque regulation for power tracking, and (3) collective pitch control for aerodynamic load management. This modular implementation enables user-configurable control strategies through parameter files, facilitating customized turbine operational protocols.

2.2. Floating platform modeling in Orcaflex

OrcaFlex demonstrates exceptional versatility in offshore engineering simulations through its advanced multi-body dynamics framework, which enables the interconnection of various representative structures such as vessels, buoys, lines, links, and winches. The software implements a comprehensive modeling suite to model the environmental and operational factors on a floater, such as current and wind loads, first-order wave excitations, wave drift damping loads, applied forces, maneuvering loads, added mass and damping coefficients, etc. These hydrodynamic parameters are typically preprocessed in third-party potential flow solvers (e.g., WAMIT or AQWA) and imported as frequency-dependent RAO datasets. For mooring system analysis, the platform incorporates dual modeling approaches: the lumped mass method idealizes lines as serially connected massless elastic segments with concentrated nodal properties, while the analytic catenary formulation provides computationally efficient static solutions. The lumped mass method is proven to be a robust and accurate method to model the flexible structures (Hall and Goupee, 2015).

OrcaFlex's nonlinear time-domain formulation resolves geometric nonlinearities, including the spatial variation of both wave loads and contact loads, as shown in Eq. (4).

$$\mathbf{M}(\mathbf{p},\mathbf{a})+\mathbf{C}(\mathbf{p},\mathbf{v})+\mathbf{K}(\mathbf{p})=\mathbf{F}(\mathbf{p},\mathbf{v},t) \tag{4}$$

where **M**, **C** and **K** respectively denote the system inertia matrix, damping matrix, and restoring stiffness matrix. **F** represents the environmental excitation forces. The state vectors **p**, **v**, **a** correspond to nodal positions, velocities, and accelerations at time *t*. Both explicit and implicit time-domain integration schemes are available. The explicit scheme uses a semi-implicit Euler method with a constant time step, solving the local equation of motion for each free body and each line node. In contrast, the implicit scheme uses the generalized-α scheme for solving the system-wide equation of motion at the end of each time step, which requires an iterative process due to the unknown values of **p**, **v**, and **a** at the end of the time step. Though the implicit scheme demands greater computational time per step, it allows substantially larger time steps compared to explicit scheme, significantly enhancing computational efficiency for long-duration simulations.

2.3. Development of OrcaWind interface

Fig. 2 presents the schematic diagram of the OrcaWind coupling framework. The implementation establishes a partitioned-domain coupling where FASTDLL resolves the aeroelastic behavior of the wind turbine with a movable tower-base interface, while Orcaflex simulates the floating platform and mooring dynamics. Crucially, the FOWT's mass distribution is exclusively resolved in OrcaFlex to ensure consistent calculation of gravitational, buoyant, inertial, and restoring forces, while aerodynamic loads from FASTDLL are applied as applied excitation forces through coordinate-transformed force vectors. At each synchronization interval, OrcaFlex receives turbine-derived aerodynamic forces in the global coordinate system and concurrently transmits platform kinematics (position/velocity/acceleration tensors) to FASTDLL. The latter computes turbine responses using its structural dynamics solver (ElastoDyn). To avoid initial imbalances between gravitational and buoyant forces, and inaccuracies in inertial force transfer due to the separate modeling of the floating platform and wind turbine and the time-lagged acceleration feedback, Orcaflex only reads the aerodynamic loads from the wind turbine. It should be noted that the mass of wind turbine is included in Orcaflex model, thus the inertial and gravitational load contributions of the wind turbine as well as the received aerodynamic loads are considered when resolving the motion equations of the floating platform. Moreover, the aerodynamic loads are based on a comprehensive aero-elastic-servo coupled wind turbine model, where the effects of platform kinematics, blade/tower flexibility, controller behavior are included.

Fig. 3 details the computational workflow implementing this staggered coupling scheme. The OpenFAST architecture is restructured into three-phase execution modules: 1) Initialization (case parameters and memory allocation), 2) Time-marching operator (aerodynamic load calculation with prescribed platform kinematics), and 3) Termination (data output and resource release). Within the time-marching phase, a shared memory buffer facilitates synchronous data exchange between

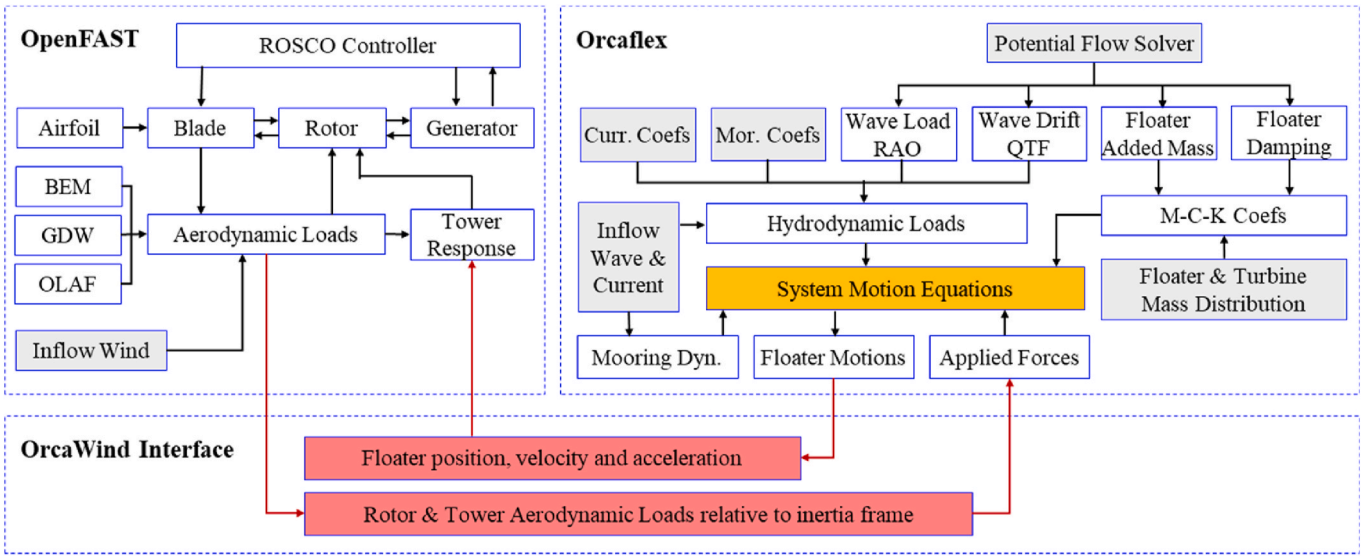

Fig. 2. Schematic diagram of the OrcaWind coupling framework.

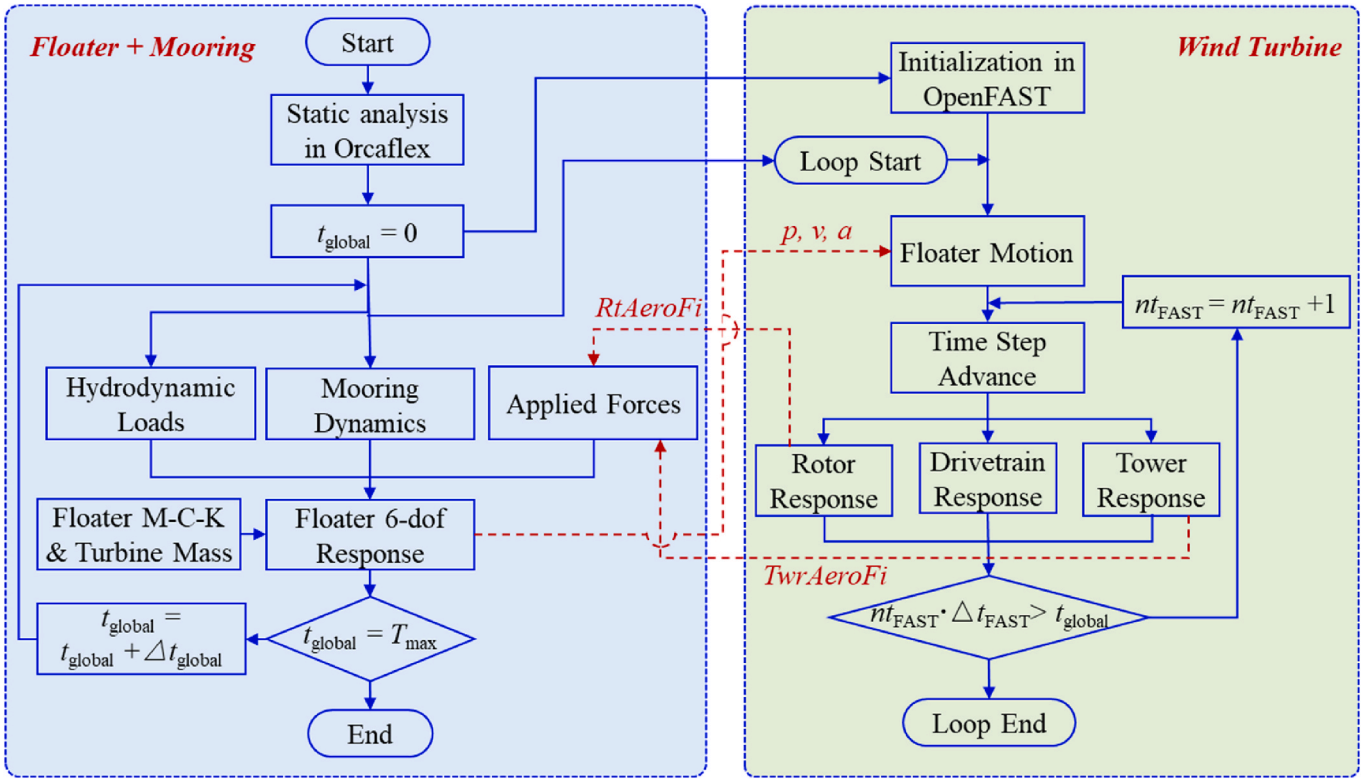

Fig. 3. Flowchart of the coupled simulation within OrcaWind framework.

solvers through pointer-referenced arrays. Notably, ElastoDyn's motion solver is modified to accept platform kinematics as boundary conditions rather than solving 6-DOF equations, effectively transforming it into a displacement-driven structural solver. Therefore, OpenFAST primarily functions as an aerodynamic load provider responding to platform kinematics within OrcaWind framework. This platform-centric approach enables Orcawind to simulate novel configurations impossible under FASTlink's turbine-centric paradigm.

OpenFAST typically operates with small fixed time steps (e.g., 0.01 s) for numerical stability, whereas Orcaflex provides both fixed-step explicit and implicit integration options. Notably, Orcaflex's implicit scheme enables substantially larger time steps (e.g., up to 0.2 s), achieving significant advantages in computational efficiency while maintaining solution stability. Since the slow-varying platform dynamics permit larger hydrodynamic steps, while rapid wind/structural responses require finer aerodynamic resolution, the co-simulation framework implements an adaptive sub-stepping scheme to address this temporal incompatibility and eliminate the need for manual step synchronization. This time-stepping scheme allows OrcaFlex's global step to encapsulate multiple FASTDLL sub-steps, with aerodynamic forces from terminal sub-step feedback into Orcaflex's external force application interface. Specifically, at each global step t_{global}, Orcaflex

solves platform motions and sends kinematics to FASTDLL. Then, FASTDLL computes aerodynamic loads over N sub-steps, with N dynamically determined by computing t_{fast} and t_{global} markers. This process achieves a two-way data exchange: updating floater kinematics in FASTDLL while feedback the rotor aerodynamic loads from the terminal sub-step into Orcaflex's force application module.

A Python-mediated coupling interface automates this synchronization while enforcing consistent SI unit conversion and proper coordinate transformation between local/global reference frames. The architecture maintains numerical stability through implicit-explicit scheme compatibility, achieving computational efficiency without compromising nonlinear dynamic fidelity.

3. Validation of the coupling framework

The computation results of the present OrcaWind framework were validated through benchmark comparisons with OpenFAST, utilizing the open-source IEA 15 MW reference wind turbine (Gaertner et al., 2020) and the VolturnUS-S semi-submersible platform (Allen et al., 2020).

3.1. Reference wind turbine and floating platform

As illustrated in Fig. 4, the IEA 15 MW turbine features a three-bladed rotor incorporating variable-speed and collective blade-pitch control. A direct-drive synchronous generator, housed within the nacelle, connects to the rotor hub. This nacelle-tower assembly is rigidly mounted on the VolturnUS-S platform. The floating platform comprises a central column triadically connected to peripheral columns via radial pontoons. The station-keeping system employs three catenary mooring lines with fairlead attachment points at the outer columns. Table 1 summarizes key design parameters for both the turbine and platform subsystems. The anchor radius is the horizontal distance from platform center to anchor.

3.2. Comparisons between OpenFAST and OrcaWind

To verify the consistency between OpenFAST and OrcaWind, identical wind turbine parameters, floating platform configurations, and environmental conditions (wind/wave inputs) were implemented. Table 2 lists the validation case matrix, where key parameters include: significant wave height (H_s), peak spectral period (T_p), JONSWAP peak enhancement factor (γ), hub-height mean wind speed (V_{hub}), turbulence intensity (TI), vertical shear exponent (PL), and design load case (DLC) classification. The environmental conditions correspond to DLC 1.1 (normal power production), representing typical operational scenarios. Pre-generated time-series files ensured synchronized wind-wave inputs, with turbulent wind fields followed the IEC Kaimal spectrum at three hub-height wind speeds (6 m/s, 12 m/s, 18 m/s) covering below-rated, near-rated, and above-rated operational conditions. Corresponding wave conditions followed the JONSWAP spectrum with $\gamma = 1.0$ and the H_s values were scaled according to the wind speed magnitudes.

To ensure hydrodynamic consistency within models, the restoring stiffness, added mass, potential damping coefficients, and the transfer functions of the first-order wave forces and wave drift forces were directly converted from OpenFAST's WAMIT-derived hydrodynamic data files (.hst, .1, .3, .12d formats) to OrcaFlex. For wind turbine modeling equivalence, both frameworks shared identical AeroDyn (aerodynamic), ServoDyn (control system), and ElastoDyn (structural dynamics) module configurations.

Table 1
Main Parameters of the reference wind turbine and platform.

Category	Parameters	Units	Values
Wind Turbine	Rated Power	MW	15
	Cut in/Rated/Cut-out Wind Speed	m/s	3/10.59/25
	Rotor Diameter/Hub Height	m	240/150
Platform	Draft/Freeboard	m	20/15
	Hull Displacement	m^3	20/206
Mass Properties	RNA Mass/Platform Mass	te	991/17839
	VCG/VCB	m	−14.94/−13.63
	$I_{xx}/I_{yy}/I_{zz}$	$kg{\cdot}m^2$	$1.25 \times 10^6/1.25 \times 10^6/2.37 \times 10^6$
Mooring System	Mooring Length/Anchor Radius	m	850/861.15
	Mooring Pretension	kN	1348.17

Table 2
Case parameters for model validation.

Items	H_s	T_p	γ	V_{hub}	TI	PL	DLC
Case A	1.5 m	5.79 s	1.0	6.0 m/s	23.0 %	0.14	1.1
Case B	2.0 m	8.52 s	1.0	12.0 m/s	18.0 %	0.14	1.1
Case C	2.7 m	10.90 s	1.0	18.0 m/s	14.5 %	0.14	1.1

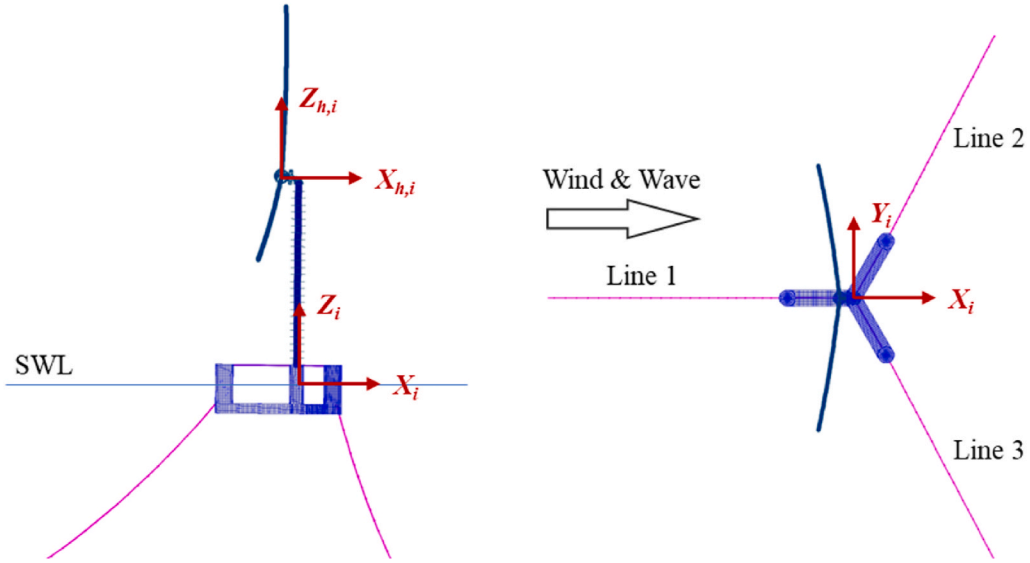

Fig. 4. The reference FOWT and the coordinate systems: (a) side view; (b) top view.

Numerical stability analysis revealed OpenFAST required a 0.01 s fixed time step, with simulations diverging at 0.02 s thresholds. The OrcaWind framework implemented a hybrid temporal scheme: OrcaFlex's implicit integration operated at 0.2 s intervals while maintaining 0.02 s aerodynamic sub-stepping for FASTDLL. During 3600-s simulations on a laptop with the CPU of AMD Ryzen @ 2.10 GHz, OpenFAST averaged 50 min per case versus OrcaWind's 28 min (44 % reduction), demonstrating enhanced computational efficiency without compromising stability.

A comparative analysis of numerical results obtained from OpenFAST and OrcaWind frameworks is presented. Considering the increased frequency of blade and rotor control actions coupled with heightened aerodynamic loading effects near rated wind speeds - factors contributing to complex FOWT dynamic responses - time-series data presentation is limited to Case B for conciseness, while statistical comparisons encompass all operational conditions.

Fig. 5 displays time-domain comparisons for Case B, illustrating (a) incoming wind speed, (b) rotor speed, (c) blade pitch angle, and (d) generator power. The wind speed (V_w), defined as the rotor-disk-averaged relative velocity perpendicular to the rotor plane, fluctuates around 12 m/s with remarkable consistency in both pattern and magnitude between two frameworks. Rotor speed maintains stability at approximately 7.5 rpm (Fig. 5b), while blade pitch angles demonstrate greater variability (4°–12° range) yet maintain synchronized trends between solutions (Fig. 5c). Generator power outputs (Fig. 5d) exhibit nearly identical fluctuations spanning 10–18 MW, confirming solution convergence.

Fig. 6 presents statistical comparisons of the evaluated parameters across all operational cases (A-C), where OF and OW denote OpenFAST and OrcaWind respectively. Quantitative analyses reveal strong agreement between the two frameworks. For instance, the V_w exhibit intercode deviations below 1.3 % across maximum, minimum, mean, and standard deviation metrics. This consistency extends to rotor dynamics (Fig. 6b), blade positioning (Fig. 6c), and power generation characteristics (Fig. 6d), with all discrepancies within acceptable thresholds (e.g., 5 %), confirming OrcaWind's computational fidelity in capturing FOWT dynamics under combined turbulent winds and irregular wave conditions. The framework's particular competence in servo-aerodynamic coupling simulation is thereby validated through comprehensive statistical verification.

Figs. 7 and 8 present temporal and statistical comparisons of aerodynamic and structural loads between the numerical frameworks. Fig. 7 demonstrates synchronized time-domain responses for rotor aerodynamic forces (RtAeroFx, Fig. 7a) and moments (RtAeroMx, Fig. 7b), confirming accurate load transfer from FASTDLL to Orcaflex. Tower base shear forces (TwrBsFx, Fig. 7c) and bending moments (TwrBsMy, Fig. 7d) maintain equivalent phase characteristics, validating structural response consistency between solvers.

Statistical comparisons in Fig. 8 reveal that the rotor thrust and torque exhibit near-identical statistical distributions, and the tower base shear forces and pitching moments show mean value deviations within 5 % relative error. However, the extremes of the tower base forces and moments demonstrate comparable magnitude differences. These discrepancies stem from OrcaWind's sequential coupling methodology, where the platform motions received by the wind turbine at each time step come from OrcaFlex's dynamic output at prior time step, inherently introducing a one-step latency. This is an inherent characteristic of partitioned-domain coupling and particularly affects tower load calculations that depend on instantaneous inertial- and gravitational-related components. The framework's strategic restriction to aerodynamic load transfer prevents error propagation from platform motions and tower base loads, thereby maintaining numerical stability without requiring acceleration prediction algorithms. This approach ensures the solution accuracy while enabling independent time-step configurations for hydrodynamic and aerodynamic computations.

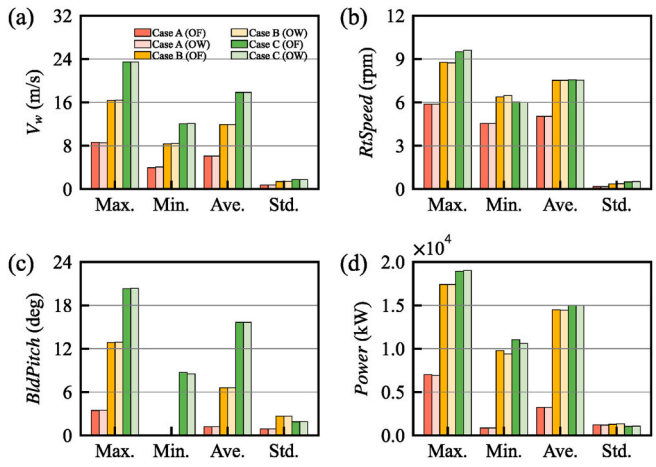

Fig. 6. Statistics of the wind velocity, rotor speed, blade pitch and power: (a) relative wind velocities; (b) rotor speed; (c) blade pitch angle; (d) generator power.

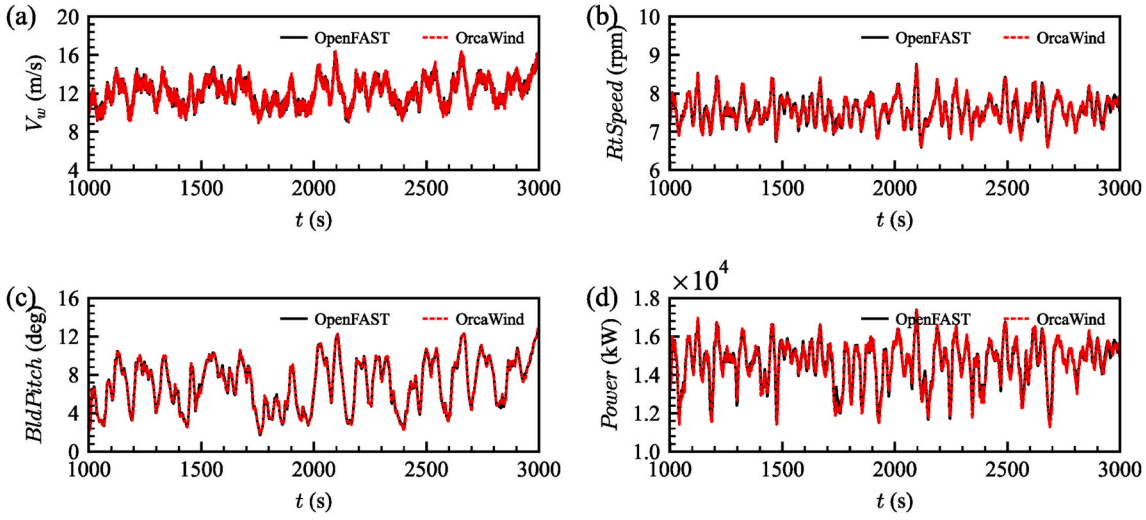

Fig. 5. Wind velocity, rotor speed, blade pitch and power under turbulent wind (V_{hub} = 12 m/s) and irregular wave (H_s = 2.0 m): (a) the x-component of rotor-disk-averaged relative wind velocities; (b) rotor speed; (c) blade pitch angle; (d) electrical generator power.

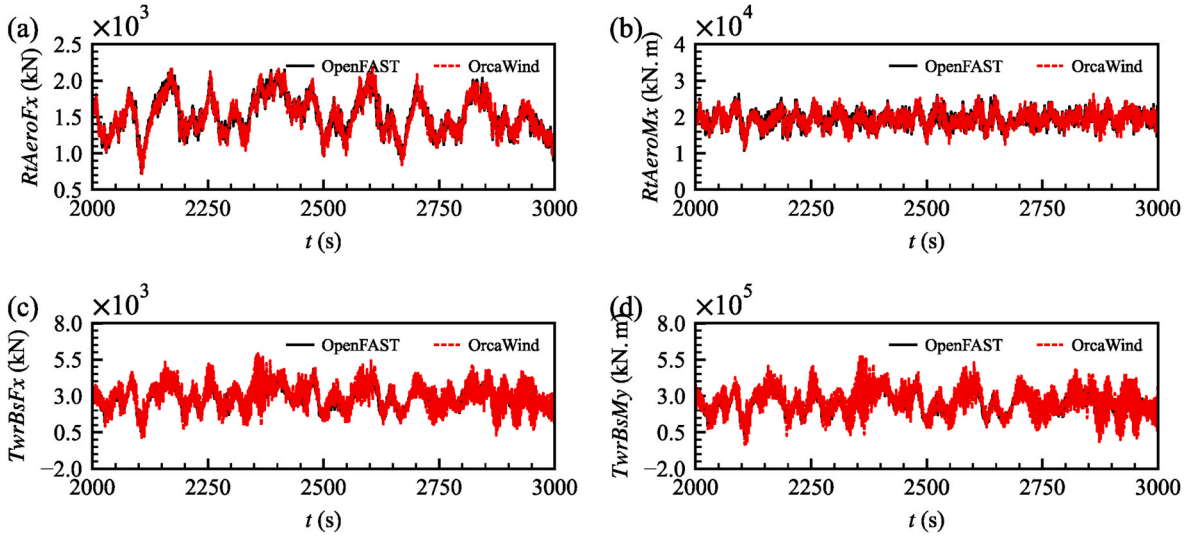

Fig. 7. Aerodynamic and tower base loads under turbulent wind (V_{hub} = 12 m/s) and irregular wave (H_s = 2.0 m): (a) the x-component of total rotor aerodynamic forces; (b) the x-component of total rotor aerodynamic moments; (c) tower base fore-aft shear force; (d) tower base pitching moment.

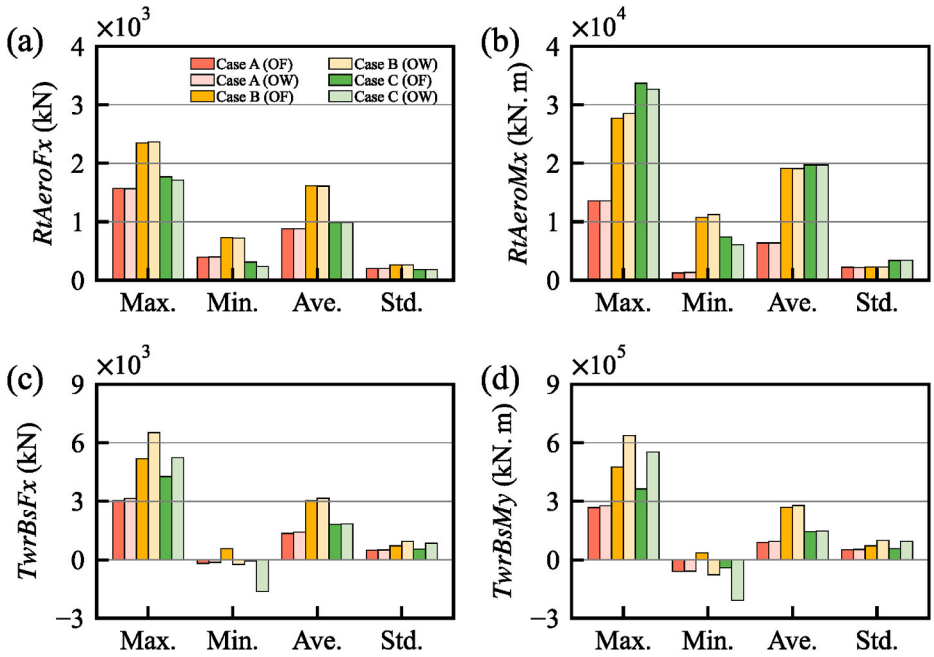

Fig. 8. Statistics of the aerodynamic and tower base loads: (a) aerodynamic forces; (b) aerodynamic moments; (c) fore-aft shear force; (d) pitching moment.

Fig. 9 compares platform responses between numerical frameworks across four degrees of freedom: surge (a), heave (b), pitch (c), and yaw (d). Fig. 9a demonstrates inter-framework agreement in capturing surge amplitude oscillations, with both solvers resolving periodic components accurately. In Fig. 9b, the heave motion is relatively small, fluctuating around 0 m with minor fluctuations, and both tools show similar patterns. Pitch responses in Fig. 9c exhibit greater dynamic ranges (0°–6°), yet maintain synchronized phase evolution throughout the simulation timeframe. Yaw rotations (Fig. 9d) display bounded oscillations (±8°), with both frameworks replicating gyroscopic coupling effects. The temporal comparisons reveal consistent amplitude-phase characteristics across all modes, confirming OrcaWind's capability in resolving coupled platform motions with fidelity comparable to OpenFAST's solutions.

Fig. 10 presents statistical comparisons of platform responses across operational cases (A-C) between OpenFAST (OF) and OrcaWind (OW). Inter-framework analyses demonstrate good statistical concordance, with surge and pitch extremes respectively exhibiting <2 % and 12 % variance in maximum values between solutions. The heave motion discrepancies are within 5 % in standard deviation values. Yaw statistics show complete parameter alignment across all metrics. The slight differences observed in some statistical values, such as the maximum pitch values, can be attributed to the pitch motion's sensitivity to the wind-induced overturning moment and the tall tower structure. Moreover, asynchronous temporal resolutions between Orcaflex and FASTDLL solvers induce phased data transfer latencies. Overall, the inter-framework statistical convergence confirms OrcaWind's equivalence in modeling FOWT hydro-aero-elastic responses, substantiating its predictive capability for offshore wind system dynamics.

Fig. 11 presents the time-series results of the mooring tensions at the fairlead. The mooring tensions from both numerical tools exhibit consistent trends in terms of phase and amplitude. In Fig. 11a, Line 1's tension fluctuates around an average value of approximately 3.7 × 10^3

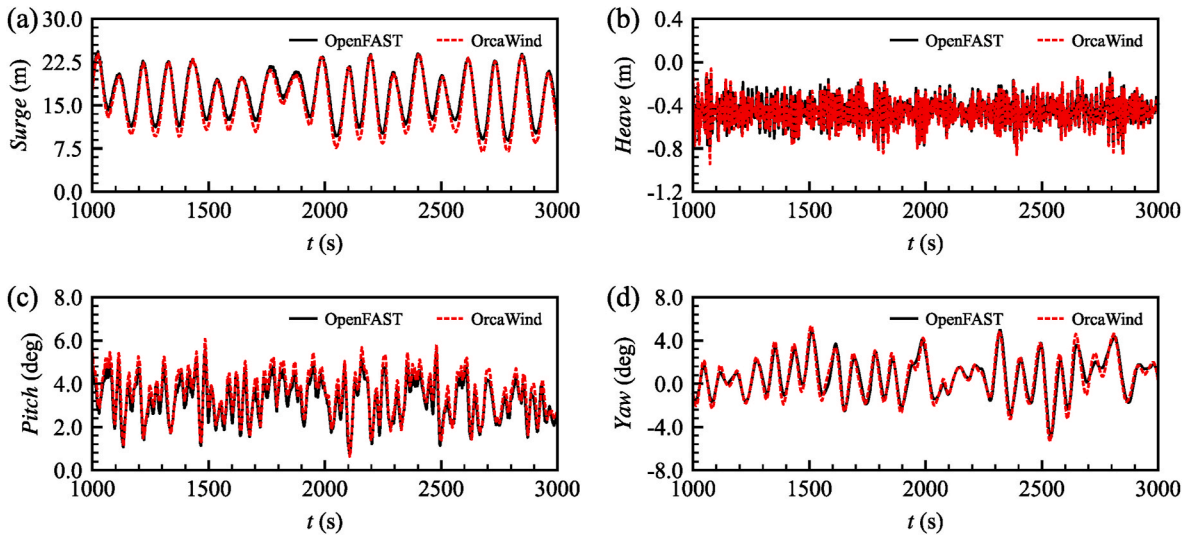

Fig. 9. Floater motions under turbulent wind (V_{hub} = 12 m/s) and irregular wave (H_s = 2.0 m): (a) surge; (b) heave; (c) pitch; (d) yaw.

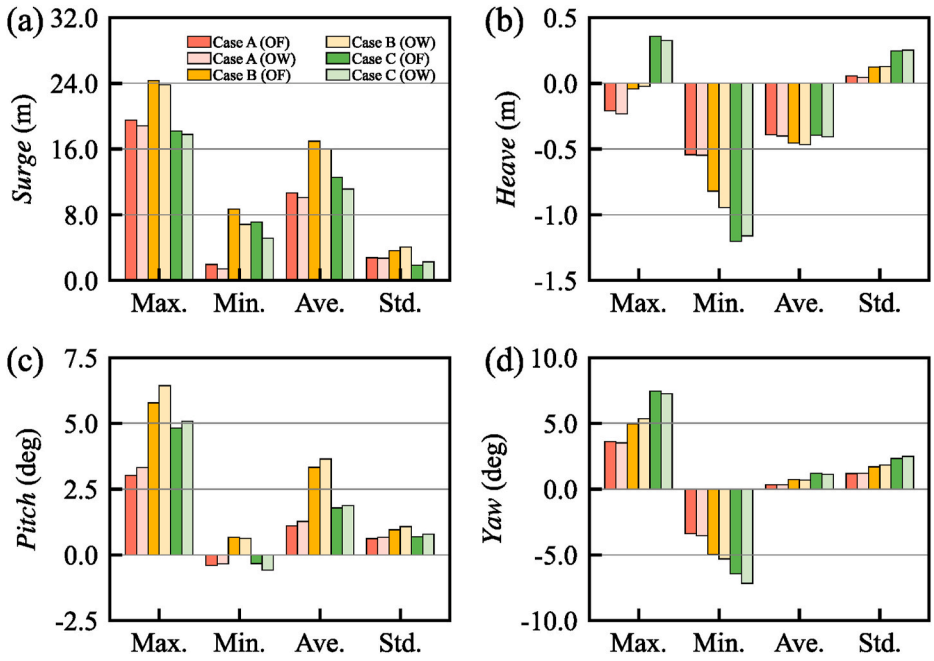

Fig. 10. Statistics of floater motion responses: (a) surge; (b) heave; (c) pitch; (d) yaw.

kN, and both OpenFAST and OrcaWind accurately capture the periodic fluctuations. In Fig. 11b and c, the tensions of Line 2 and Line 3 exhibit similar patterns, with average values of about 2.1 × 10^3 kN. The slight amplitude differences between the two frameworks are insignificant and do not influence the overall trend, indicating that the OrcaWind framework can reliably reproduce the mooring tension responses. Fig. 12 shows the statistical results of the mooring tensions for the three lines. The maximum, minimum, average, and standard deviation values from both numerical tools are nearly identical, further validating the reliability of the OrcaWind framework.

In summary, the comprehensive comparison between OrcaWind and OpenFAST across multiple operational conditions confirms the accuracy and reliability of OrcaWind in predicting FOWT coupled dynamic responses. The framework demonstrates consistent performance in simulating control behaviors, aerodynamic loads, platform motions, and mooring tensions when benchmarked against OpenFAST. Observed discrepancies in platform motion responses primarily stem from asynchronous data transfer between Orcaflex and FASTDLL. These deviations remain within acceptable engineering tolerances. The development and validation of OrcaWind effectively integrate OpenFAST's wind turbine modeling capabilities with OrcaFlex's floating platform and mooring system simulation strengths, enabling accurate and efficient analysis of diverse FOWT configurations. The subsequent section will demonstrate OrcaWind's unique capabilities through dynamic analysis of an innovative mooring system design for the IEA 15 MW wind turbine.

4. Case study: 15 MW FOWT with constant tension mooring system (CTMS)

This section leverages the unique capability of OrcaWind by presenting a case study focusing on a 15 MW FOWT equipped with an innovative CTMS. Such configurations pose significant modeling challenges due to the complex, nonlinear interactions between the floater

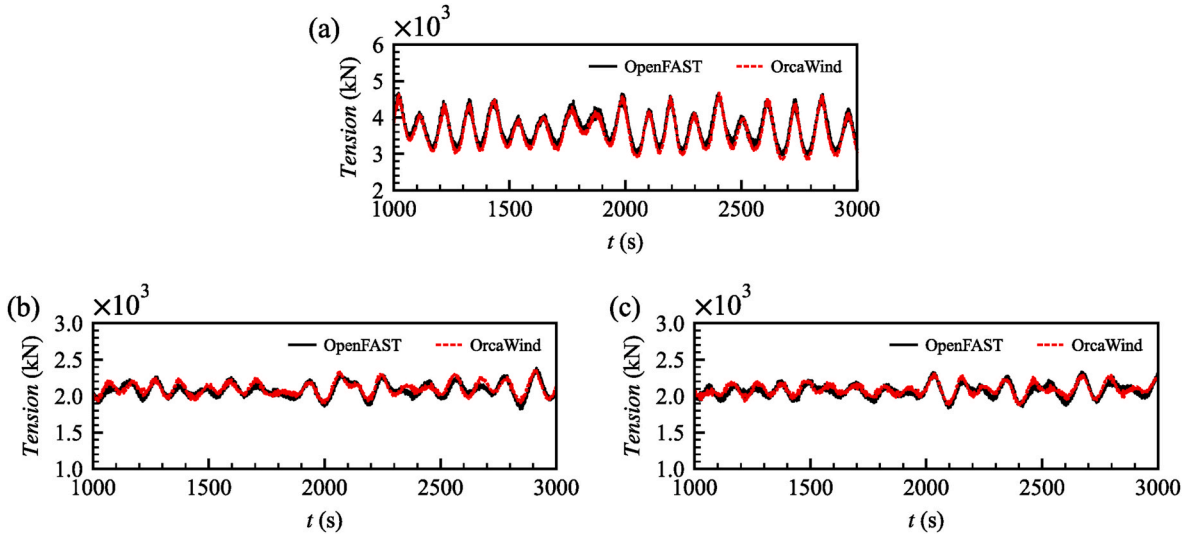

Fig. 11. Fairlead tensions of the mooring lines under turbulent wind (V_{hub} = 12 m/s) and irregular wave (H_s = 2.0 m): (a) Line 1; (b) Line 2; (c) Line3.

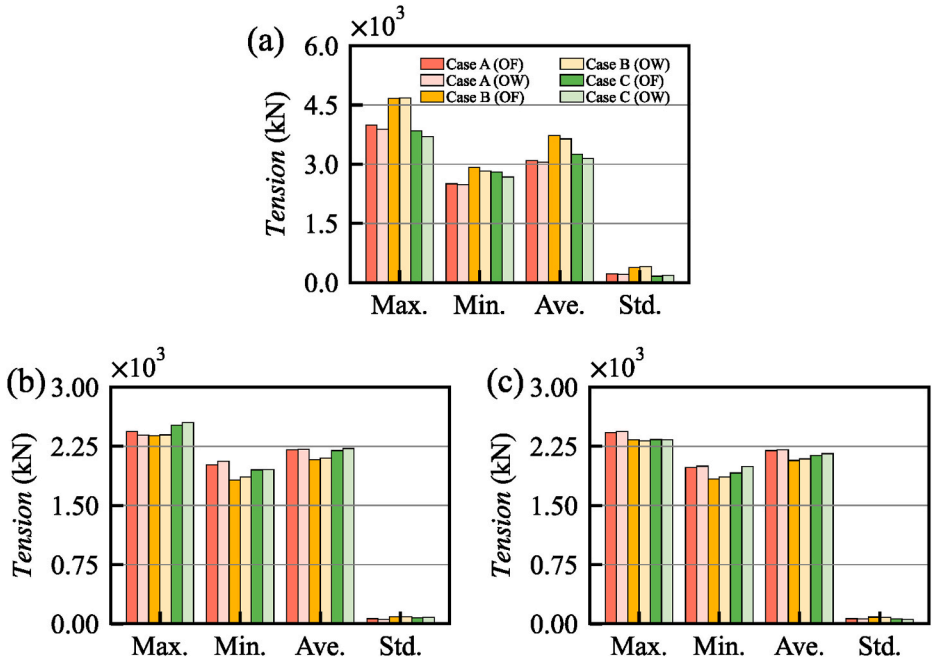

Fig. 12. Statistics of fairlead tensions of the mooring lines: (a) Line 1; (b) Line 2; (c) Line3.

and the mooring components like clump weights and winch wires.

4.1. CTMS configuration

This investigation examines the dynamic responses of a 15 MW FOWT integrated with a CTMS(Wang et al., 2023). The CTMS is expected to mitigate abrupt tension surges observed in conventional catenary configurations under intermediate water depths. As illustrated in Fig. 13, the system comprises a clump weight and winch wires. It releases kinetic energy by increasing the platform's movement distance, maintaining the instantaneous peak tensions below the chain's breaking strength. The clump weight's mass is distributed across three mooring lines. An auxiliary chain with fixed length connects Fairlead 5 to the clump weight, preventing seabed contact during calm and moderate sea conditions. This adaptation streamlines numerical modeling while enabling cross-validation through simplified OpenFAST simulations. Key CTMS parameters are listed in Table 3, where L_d denotes the baseline chain length between Fairlead 5 and the clump weight, EA denotes the axial stiffness of the mooring chain material. It should be noted that the mooring line length denotes the unstretched chain segment length from the fairlead to the anchor point, while the anchor radius is the horizontal distance from the floating platform's center to the anchor position.

4.2. Mooring system modeling

The OrcaFlex models the platform-penetrating wires through winch objects, with chain and clump weight connections at each termination. Multiple frictionless fairleads enable smooth winch wire transitions. For OpenFAST compatibility, an equivalent-stiffness approximation replaces the physical winch-weight mechanism. Line 1 (primary load-bearing line) employs a nonlinear tension-strain relationship, while

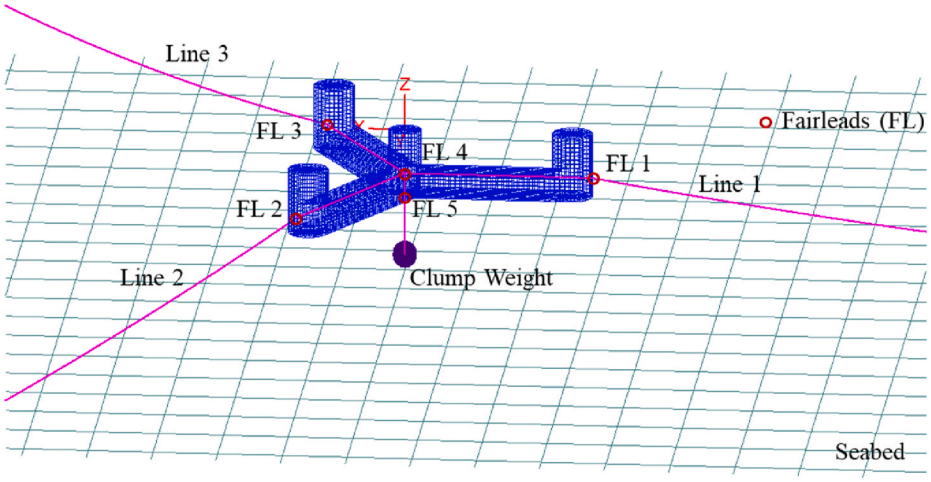

Fig. 13. The Orcaflex model of the 15 MW FOWT with CTMS.

Table 3
Mooring parameters for the reference constant tension mooring system.

Water Depth	Length	Anchor radius	Fairlead Height	Clump weight in water	*Ld*	Chain Diameter	*EA*
45 m	650 m	698.8 m	−14 m	300 te	22 m	0.333 m	3.27×10^6kN

Lines 2 and Line 3 (leeward lines with minimal clump weight support loads) retain constant stiffness coefficients.

The OpenFAST model implements a triphasic stiffness adaptation for Line 1's *EA* value, as depicted in Fig. 14. The stiffness initially maintains baseline stiffness (EA_0) when mooring tensions remain below the clump weight's submerged weight, followed by controlled stiffness attenuation when tensions surpass this threshold to limit load escalation rates. Beyond 3 % strain, stiffness restoration activates to prevent clump weight-platform collisions while progressively recovering nominal *EA* characteristics. This nonlinear parametrization prevents numerical instabilities arising from non-unique tension-strain mappings and avoid unphysical line elongation along with the constant-tension assumptions.

Wang et al. (2023) analyzed the CTMS dynamic behavior during parked operations under extreme environmental conditions. Both the CTMS and the parked turbine were modeled in Orcaflex. Table 4 details the environmental parameters for this case, examining the IEA 15 MW FOWT with CTMS under 50-year return period waves combined with near-rated wind inflow. This condition represents DLC1.6 status characterized by normally operating wind turbine in severe sea state. The wave spectral parameters align with the specifications in Wang et al. (2023), while the wind speed marginally exceeds the rated wind speed. Within the OrcaWind framework, the CTMS and the operating turbine were modeled in Orcaflex and OpenFAST, respectively.

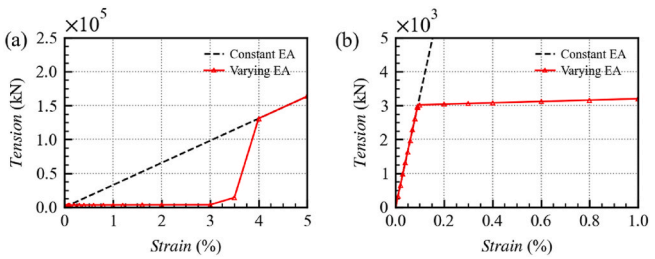

Fig. 14. The EA model of constant tension mooring system adopted in OpenFAST: (a) overall view; (b) zoomed-in view.

Table 4
Wave and wind parameters for case study.

H_s	T_p	γ	V_{hub}	*TI*	*PL*	DLC
10.7 m	14.2 s	2.75	12.0 m/s	18 %	0.14	1.6

4.3. Dynamic responses of the FOWT system

Fig. 15 compares platform motion time-histories between frameworks. Both solutions capture consistent motion trends, with heave responses (least mooring-sensitive DOF) demonstrating superior agreement in amplitude-phase synchronization. Surge motions (most mooring-dependent DOF) exhibit greater deviations, attributable to OpenFAST's simplified mooring modeling limitations in resolving CTMS interaction complexities.

Fig. 16 quantifies motion statistical divergences. Surge parameters show the largest discrepancies: OpenFAST underpredicts maximum surge by 31 % and standard deviation by 16 % relative to OrcaWind, evidencing systemic underestimation of mooring-coupled responses.

Fig. 17 analyzes motion power spectral densities (PSDs). OpenFAST exhibits notable low-frequency simulation errors, particularly for mooring-dominated surge (Fig. 17a) and pitch (Fig. 17c) DOFs, displaying attenuated spectral peaks. It is noted that this spectral divergence stems from its quasi-static mooring approximation when modeling unconventional configurations like CTMS, not fundamental algorithm. It underscores the necessity of high-fidelity coupling approaches like OrcaWind for CTMS-equipped FOWTs. Compared to conventional systems, CTMS configurations exhibit amplified wave-frequency contributions in surge/pitch responses due to the system's variable-length mooring geometry imposing reduced wave-motion constraints.

Fig. 18 compares mooring tension time histories between the numerical frameworks. Despite satisfactory platform motion agreement, significant tension discrepancies emerge. For Line 1 (Fig. 18a), OpenFAST simulations show peak tensions approximating the clump weight's submerged weight, while OrcaWind predicts marginally reduced peaks due to load redistribution through Lines 2–3's slack segments. Although both frameworks capture comparable tension trends, OpenFAST

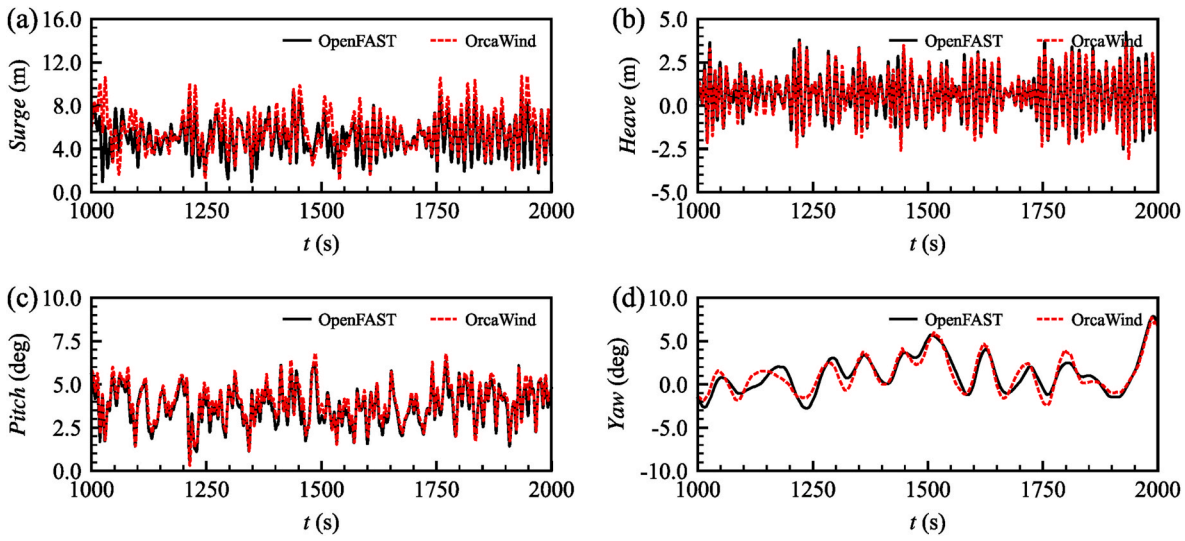

Fig. 15. Floater motion responses of the 15 MW FOWT with constant tension mooring system: (a) surge; (b) heave; (c) pitch; (d) yaw.

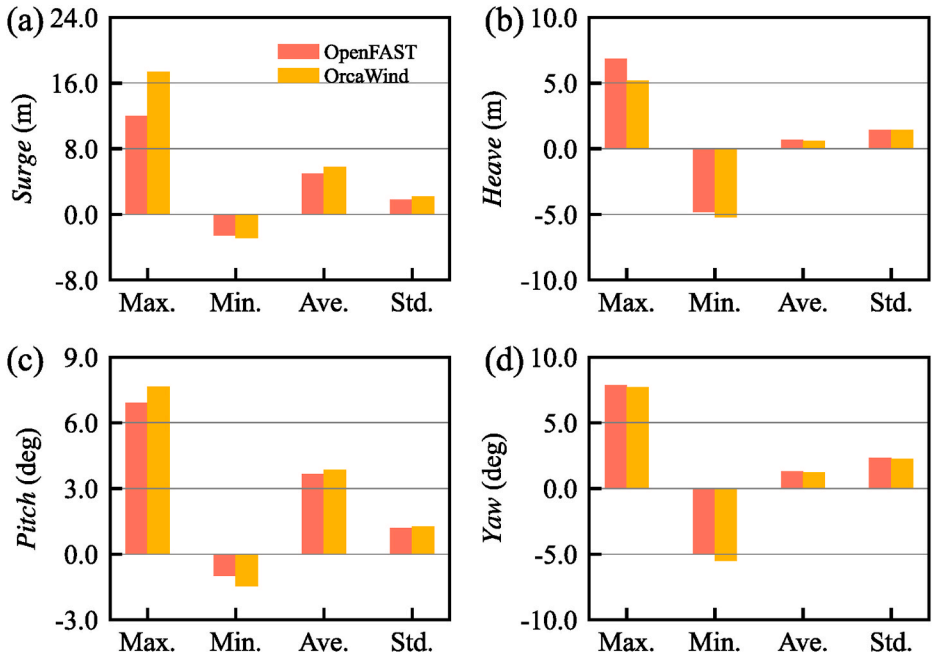

Fig. 16. Statistics of floater motion responses of the 15 MW FOWT with constant tension mooring system: (a) surge; (b) heave; (c) pitch; (d) yaw.

exhibits unphysical zero-tension troughs - artifacts of strain-based tension interpolation when loads fall below clump weight thresholds. Lines 2 and Line 3 tensions (Fig. 18b and c) demonstrate phase synchronization but amplitude mismatches. OrcaWind's predictions average 5–7 % lower than OpenFAST's, reflecting its superior capability in modeling slack line conditions during clump weight elevation - a physical phenomenon unaccounted for in OpenFAST's simplified approach. This modeling limitation causes overestimation of line tensions for Line 2 and Line 3 in the OpenFAST framework. While both MoorDyn and OrcaFlex utilize lumped mass formulations, OpenFAST's structural solver restrictions required approximating the CTMS counterweight-pulley system as a fixed-length mooring system with varying *EA* parameter. OrcaFlex natively resolves dynamic interactions between moving parts, validating its superior capability for novel mooring topologies.

The comparative results further validate the OrcaWind framework's reliability in simulating coupled FOWT dynamics. While OpenFAST achieves reasonable platform motion predictions through stiffness-equivalent approximations, its surge motion and mooring tension errors critically compromise mooring fatigue assessments. This simplified approach inherently neglects tri-line load distribution mechanisms and proves inadequate under misaligned wind-wave-current conditions.

5. Conclusions

This study developed and validated OrcaWind, an advanced aero-hydro-servo-elastic coupling framework integrating OpenFAST and OrcaFlex, to address critical limitations in simulating FOWT dynamics. Key findings are summarized as follows.

(1) OrcaWind effectively integrates OpenFAST's robust aero-elastic-servo modeling capabilities with OrcaFlex's advanced hydrodynamic and mooring system modeling, creating a powerful combined solution. This enables comprehensive simulations of FOWT

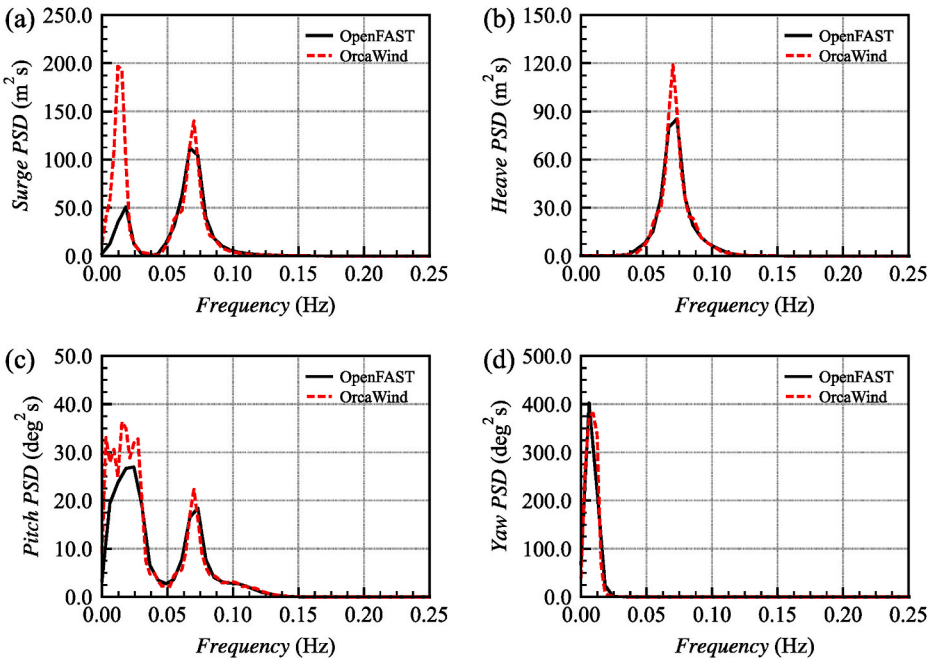

Fig. 17. Power spectral densities of floater motion responses of the 15 MW FOWT with constant tension mooring system: (a) surge; (b) heave; (c) pitch; (d) yaw.

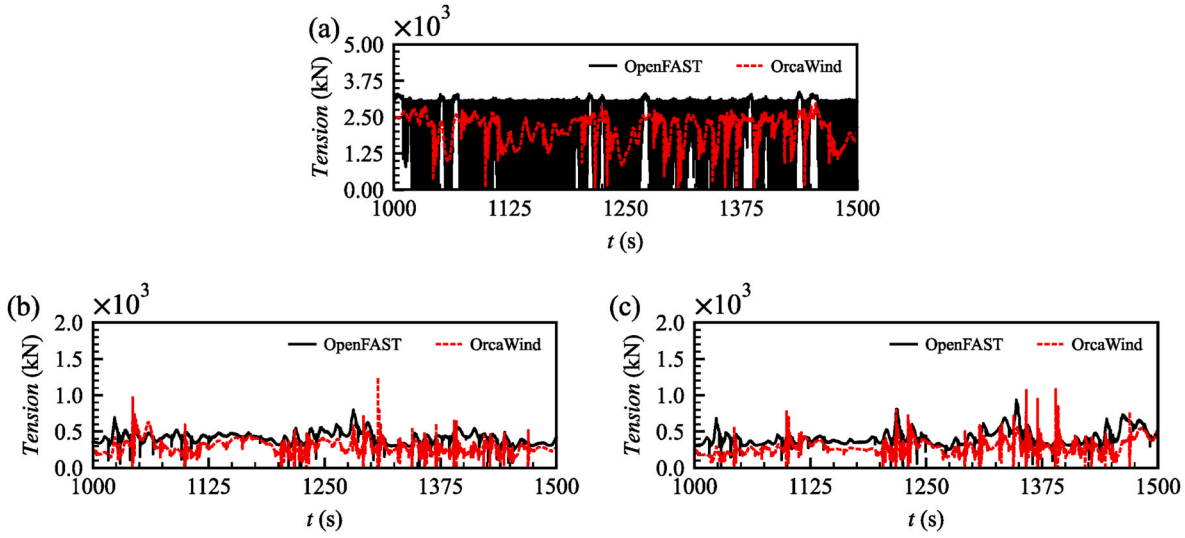

Fig. 18. Fairlead tensions of the constant tension mooring system under turbulent wind and irregular wave condition: (a) Line 1; (b) Line 2; (c) Line3.

dynamics, overcoming the single-tool limitations in existing approaches.

(2) Comparative analyses with OpenFAST confirm OrcaWind's reliability in predicting servo-control responses, aerodynamic loads, platform motions, and mooring tensions. The minor discrepancies in tower base loads primarily originate from the sequential data-exchange mechanism of partitioned-domain coupling.

(3) The 15 MW FOWT case study with a CTMS highlights OrcaWind's unique advantage in handling innovative designs. Unlike OpenFAST's oversimplification in the mooring lines system, the framework accurately resolves nonlinear interactions between floating platform and complex mooring configurations.

OrcaWind provides researchers and engineers with an efficient tool for FOWT design optimization, particularly for systems involving novel substructures or mooring solutions. Future efforts will extend the framework's capabilities to multi-rotor turbine and shared mooring systems of wind farm, thereby enhancing cost-effective design optimization for commercial-scale floating wind farms.

CRediT authorship contribution statement

Yanfei Deng: Writing – original draft, Conceptualization. **Cuizhi Zhu:** Writing – review & editing. **Sara Ying Zhang:** Formal analysis, Data curation. **Yifeng Yang:** Validation, Methodology. **Bingfu Zhang:** Visualization.

Declaration of competing interest

The authors declare that they have no known competing financial interests or personal relationships that could have appeared to influence the work reported in this paper.

Acknowledgment

This work was financially supported by National Natural Science Foundation of China (52301317), Guangdong Basic and Applied Basic Research Foundation (2024A1515011587), Guangdong Provincial Department of Science and Technology's Guangdong-Hong Kong-Macao Joint Innovation Project (No. 2024A0505040006), Shenzhen Science and Technology Program (JCYJ20240813110411016) and Guangdong Provincial Special Funds for Marine Economic Development (GDNRC [2023]48). These sources of support are gratefully acknowledged.

References

Allen, C., Viscelli, A., Dagher, H., Goupee, A., Gaertner, E., Abbas, N., Hall, M., Barter, G., 2020. Definition of the Umaine VolturnUS-S Reference Platform Developed for the IEA Wind 15-megawatt Offshore Reference Wind Turbine. National Renewable Energy Lab.(NREL), Golden, CO (United States).

Bae, Y.H., Kim, M.H., 2014. Aero-elastic-control-floater-mooring coupled dynamic analysis of floating offshore wind turbine in maximum operation and survival conditions. J. Offshore Mech. Arctic Eng. 136 (2).

Bolat, F.C., Ozbek, K., Gelis, K., Erturk, E., Alujevic, N., Ozyurt, O., Sivrioglu, S., 2025. Assessing analysis of a small-scale dual rotor counter-rotation wind turbine with a unique pitch mechanism: experimental parametric study. Mech. Syst. Signal Process. 225, 112292.

Deng, Y., Zhang, S.Y., Zhang, M., Gou, P., 2023. Frequency-dependent aerodynamic damping and its effects on dynamic responses of floating offshore wind turbines. Ocean Eng. 278, 114444.

DNV, 2022. Energy Transition Outlook 2022: a Global and Regional Forecast to 2050.

Enerdata, 2023. China Starts Building a 1 GW Floating Offshore Wind Project in Hainan.

Faraggiana, E., Giorgi, G., Sirigu, M., Ghigo, A., Bracco, G., Mattiazzo, G., 2022. A review of numerical modelling and optimisation of the floating support structure for offshore wind turbines. J. Ocean Eng. Mar. Energy 8 (3), 433–456.

Gaertner, E., Rinker, J., Sethuraman, L., Zahle, F., Anderson, B., Barter, G., Abbas, N., Meng, F., Bortolotti, P., Skrzypinski, W., 2020. Definition of the IEA 15-megawatt Offshore Reference Wind Turbine.

Guo, F., Gao, Z., Schlipf, D., 2024. TorqTwin—An open-source reference multibody modeling framework for wind turbine structural dynamics. Renew. Energy 235, 121268.

Hall, M., Goupee, A., 2015. Validation of a lumped-mass mooring line model with DeepCwind semisubmersible model test data. Ocean Eng. 104, 590–603.

Hau, E., 2013. Offshore wind energy utilisation. In: Hau, E. (Ed.), Wind Turbines: Fundamentals, Technologies, Application, Economics. Springer Berlin Heidelberg, Berlin, Heidelberg, pp. 677–718.

Jonkman, J.M., Hayman, G.J., Jonkman, B.J., Damiani, R.R., Murray, R.E., 2015. Aerodyn v15 User's Guide and Theory Manual. NREL Draft Report, p. 46.

Lamei, A., Hayatdavoodi, M., Riggs, H.R., Ertekin, R.C., 2025. Wave–current–wind interaction with elastic floating offshore wind turbines. Eng. Anal. Bound. Elem. 171, 106052.

Lauria, A., Loprieno, P., Francone, A., Leone, E., Tomasicchio, G.R., 2024. Recent advances in understanding the dynamic characterization of floating offshore wind turbines. Ocean Eng. 307, 118189.

Lei, Z., Wang, X., Zhou, S., Wang, Z., Wang, T., Yang, Y., 2021. A review of research status and scientific problems of floating offshore wind turbines. Energy Eng. J. Assoc. Energy Eng. 119 (1), 123–143.

Leimeister, M., 2022. Floating offshore wind turbine systems. In: Leimeister, M. (Ed.), Reliability-Based Optimization of Floating Wind Turbine Support Structures. Springer International Publishing, Cham, pp. 45–68.

López-Queija, J., Sotomayor, E., Jugo, J., Aristondo, A., Robles, E., 2024. A novel python-based floating offshore wind turbine simulation framework. Renew. Energy 222, 119973.

Luan, C., Gao, Z., Moan, T., 2017. Development and verification of a time-domain approach for determining forces and moments in structural components of floaters with an application to floating wind turbines. Mar. Struct. 51, 87–109.

Masciola, M., Robertson, A.N., Jonkman, J.M., Driscoll, F.R., 2011. Investigation of a FAST-OrcaFlex coupling module for integrating turbine and mooring dynamics of offshore floating wind turbines. In: International Conference on Offshore Wind Energy and Ocean Energy. Beijing, China.

Moriarty, P.J., 2005. AeroDyn theory manual. Techn. Rep. NREL/TP-500-36881.

NREL, 2021. OpenFAST documentation. Release v2.4.0 ed. Jan. 11, 2021. [Online]. Available: https://openfast.readthedocs.io/en/v2.4.0.

Orcina, 2023. Fastlink. Orcina.

Otter, A., Murphy, J., Pakrashi, V., Robertson, A., Desmond, C., 2022. A review of modelling techniques for floating offshore wind turbines. Wind Energy 25 (5), 831–857.

Shen, X., Li, X., Yin, F., Huang, Z., Ye, Z., Guo, X., 2024. The influence of the rotor spacing distance and rotating speed ratio on the power production of dual rotor wind turbines using a modified two-way interaction blade element momentum method. Energy 311, 133274.

Terrero-Gonzalez, A., Dai, S., Papadopoulos, J., Neilson, R.D., Kapitaniak, M., 2024. Nonlinear analysis of hydrodynamics of a shallow-draft floating wind turbine. Nonlinear Dyn.

Tian, Z., Shi, W., Li, X., Park, Y., Jiang, Z., Wu, J., 2025. Numerical simulations of floating offshore wind turbines with shared mooring under current-only conditions. Renew. Energy 238, 121918.

Wang, K., Chu, Y., Huang, S., Liu, Y., 2023. Preliminary design and dynamic analysis of constant tension mooring system on a 15 MW semi-submersible wind turbine for extreme conditions in shallow water. Ocean Eng. 283, 115089.

Xie, L., Li, C., Yue, M., He, H., Jia, W., Liu, Q., Xu, Z., Fan, L., Bashir, M., Yan, Y., 2024. Dynamic analysis of an improved shared moorings for floating offshore wind farm. Renew. Energy 232, 120963.

Xie, S., Li, Y., Li, Y., Kan, Y., 2025. Preliminary study of the dynamics and environmental response of multiple floating offshore wind turbines on a single large-scale platform. Ocean Eng. 316, 120008.

Yang, Y., Bashir, M., Michailides, C., Li, C., Wang, J., 2020. Development and application of an aero-hydro-servo-elastic coupling framework for analysis of floating offshore wind turbines. Renew. Energy 161, 606–625.